ELSEVIER

Journal of Nuclear Materials 298 (2001) 280–290

journal of nuclear materials

www.elsevier.com/locate/jnucmat

Use of UO_2 films for electrochemical studies

F. Miserque [a,b], T. Gouder [a,*], D.H. Wegen [a], P.D.W. Bottomley [a]

[a] *European Commission, JRC, Institute for Transuranium Elements, P.O. Box 2340, 76125 Karlsruhe, Germany*
[b] *Facultés Universitaires Notre-Dame de la Paix, 61 rue de Bruxelles, B-5000 Namur, Belgium, Germany*

Received 28 February 2001; accepted 4 July 2001

Abstract

UO_2 films have been prepared by dc reactive sputtering of a uranium metal target in an Ar/O_2 atmosphere. We have used the films deposited on gold substrates as working electrodes for electrochemical investigations as simulating the surfaces of fuel pellets. Film composition was determined by photoelectron spectroscopy (XPS and UPS) and X-ray diffraction (XRD). The oxide stoichiometry as a function of deposition conditions was determined and the appropriate conditions for $UO_{2.0}$ formation established. AC impedance and cyclic voltammetry measurements were performed. A double RC electrical equivalent circuit was used to fit the data from impedance measurements, similar to those used in unirradiated UO_2 or spent fuel pellets. However due to the porosity or adhesion defects on the thin films that permitted a direct contact between the solution and the gold substrate, we were obliged to add a contribution simulating the water–gold system. Cyclic voltammetry measurements show the influence of pH on the dissolution mechanism. Alkaline solutions permit the formation of an oxidised layer ($UO_{2.33}$) which is not present in the acidic solutions. In both pH = 2 and pH = 6 solutions, a U^{VI} species layer is formed. © 2001 Published by Elsevier Science B.V.

1. Introduction

Assessment of the long-term storage properties of nuclear waste in final storage repositories requires an understanding of the chemical interaction of the waste with the surrounding environment. In particular corrosion and leaching reactions, which may occur following contact with groundwater, have to be considered. Spent fuel is a complex system, composed mainly of an actinide oxide matrix (UO_{2+x}, $(U,Pu)O_{2+x}$), containing small amounts of fission products (e.g. Cs, Pd, I, etc.), which may all have an influence on its reactivity [12]. In a pragmatic approach, the dissolution behaviour of the UO_2 matrix has been studied thoroughly by electrochemical techniques [1–3] for modelling and understanding the effects of groundwater in contact with complex nuclear fuel. In the first step, simple UO_2 model electrodes in various aqueous environments were examined [4–6] and yielded detailed information about the surface oxidation and dissolution processes. Later, spent fuel systems were investigated in leaching [7,8] and electrochemical [9–11] studies. While being more representative of the realistic scenario, the results are complex and make a full understanding difficult.

To bridge the gap between the simple model and the complex real systems we have studied films of intermediate complexity, starting with simple UO_2. Variation of a small and well-defined set of parameters (e.g., Cs, Pd, O content) permits us to perform single effect studies. The films are prepared by co-deposition methods, where the actinide oxide film is doped with different fission products. Modern preparation techniques are versatile, allowing a large number of films to be prepared and studied in situ.

As the starting point we studied the electrochemical behaviour of UO_2 films. In particular we wanted to compare our results to those obtained on pellets to show that, for the same material, film and bulk samples give the same results. Starting with a simple system permits us to verify that the electrochemistry of a film UO_2 electrode can be fitted to the same dissolution model as that developed by Shoesmith and Sunder [2] based on electrochemical investigations using unirriadiated UO_2

* Corresponding author. Tel.: +49-7247 951243; fax: +49-7247 951593.
E-mail address: gouder@itu.fzk.de (T. Gouder).

0022-3115/01/$ - see front matter © 2001 Published by Elsevier Science B.V.
PII: S0022-3115(01)00650-X

electrodes. Also we are interested in the film deposition process itself, and in particular in the relation between oxide stoichiometry and deposition conditions. This is particularly important for uranium oxides, which exist in different compositions (UO_2, U_4O_9, U_3O_8, UO_3) [13,14]. Reactive sputtering allows us to prepare samples of well-defined and controlled stoichiometries, and with the possibility to change them [15]. In future, the complexity of the film will be increased by doping with selected fission products (e.g., Cs, Pd) to investigate their individual effects on the behaviour of spent fuel.

2. Experimental

UO_2 films were prepared by reactive dc sputtering of a U metal target. The plasma in the diode source was maintained by injection of electrons of 50–100 eV energy. We used ultrahigh purity Ar (99.9999%) as sputter gas. The composition of the Ar/O_2 mixture was varied to control the oxygen stoichiometry of the UO_2 film. The U target was a commercial (99.9%) U metal disc, cleaned by mechanical polishing and nitric acid etching before introduction to the vacuum chamber. The background pressure in the preparation chamber was 3×10^{-9} mbar.

Various film–substrate systems were used in this study. For the surface spectroscopy experiments, where a surface layer of 1–2 nm is analysed, films of 5 nm thickness were deposited on single crystalline Si wafers. Electrochemistry experiments were performed on films of about 1 μm thickness, deposited on polycrystalline gold discs of 10 mm diameter (0.25 mm thickness, 99.99 % purity). The thickness of the film was checked by weight difference before and after sputter deposition. XRD measurements were done on films of 1 μm. Glass was used as the substrate to avoid a contribution from a crystalline substrate.

XPS and UPS spectra were recorded using a Leyboldt LHS-10 hemispherical analyser. XPS spectra were taken using Mg K_α (1253.6 eV) radiation with an approximate energy resolution of 1 eV. UPS measurements were made using HeII (40.81 eV) excitation radiation produced by a windowless UV rare gas discharge source. The total resolution in UPS was 0.1–0.05 eV for the high resolution scans. The background pressure in the analysis chamber was 2×10^{-10} mbar.

For electrochemical measurements, a three electrode set-up was used with the UO_2 thin film on gold as working electrode. To improve the adhesion of the film, deposition was carried out at high temperature (573 K). As auxiliary electrode we used a platinum foil mounted on a Pt wire. The reference electrode was a Ag/AgCl (3 M KCl, WTW, type R302) electrode, with a potential of $+207 \pm 15$ mV vs. standard hydrogen electrode (SHE).

AC impedance measurements were recorded using the IM6 system distributed by Zahner Elektrik. The impedance was measured over the frequency range from 10^6 Hz down to 10^{-4} Hz with sine wave amplitude of 20 mV_{pp}. IMPEDANZ software written by one of the authors (D.W.) was used for equivalent circuit modelling of the results.

Free corrosion potential and cyclic voltammetry studies were carried out using a Sycopel AEW-1000 potentiostat, with data collection performed using commercial software from Sycopel Scientific. All electrochemical measurements were conducted in aerated and stirred solutions.

3. Results and discussion

3.1. XPS, UPS and XRD measurements

In this section, we describe the preparation of the UO_2 films by dc reactive sputtering and the determination of film composition using XPS, UPS and XRD techniques. Fig. 1 shows the evolution of U-4f core level spectra of UO_2 films deposited at room temperature for increasing the oxygen partial pressure. In a pure argon plasma, the U-4f spectrum is typical for metallic uranium, characterised by the sharp and asymmetrical

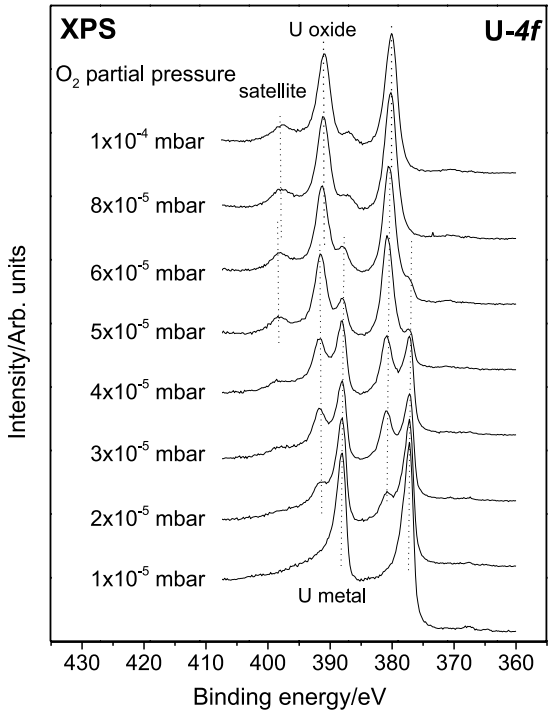

Fig. 1. XPS-U-4f study of UO_x as a function of O_2 partial pressure.

spin-orbit split U-4f$_{7/2}$ and U-4f$_{5/2}$ lines at 377.0 and 388.0 eV, respectively, [16]. The line asymmetry indicates a high density of states (DOS) at the Fermi level (E_F), mainly attributed to the U-5f states. For an oxygen partial pressure of 2×10^{-5} mbar, additional peaks appear at 380.8 eV (U-4f$_{7/2}$) and 391.7 eV (U-4f$_{5/2}$), indicating the formation of substoichiometric UO_2 (UO_{2-x}) [17]. It should be added that the precise relationship between oxide composition and oxygen pressure depends on the experimental set-up, e.g., the sputter rate or target–substrate distance. Absolute O_2 pressure should thus not be taken as universal reference. With increasing oxygen partial pressure, the oxide signal increases in intensity, replacing the metal signal, thus indicating further oxidation of the film. For an oxygen pressure of 6×10^{-5} mbar negligible metallic peaks remain, thus indicating complete oxidation. At even higher pressure the U-4f oxide lines shift to a lower binding energy by about 1 eV. This shift is due to the further oxidation of UO_{2-x} into stoichiometric UO_2. Since this oxidation results in the transformation of the n-type UO_{2-x} semiconductor into p-type UO_2 or UO_{2+x}, the accompanying decrease in the Fermi energy causes a shift of the entire spectrum [17]. Formation of UO_2 is further shown by the presence of shake-up satellites at 6.7 eV higher binding energy than the main U-4f lines [18].

The valence band studies shown in Fig. 2 confirm the U-4f core level results. In the absence of oxygen, the valence band spectrum exhibits an intense peak at E_F attributed mainly to 5f states, characteristic for metallic uranium [16]. With increasing partial pressure the intensity of the U-5f peak at E_F decreases, which is ascribed to the oxidation of U metal, until it disappears at 5×10^{-5} mbar. This is practically the same pressure at which the U-4f lines show complete replacement of U metal by the oxide. Increasing oxygen pressure further results in the strengthening of a broad band between 4 and 8 eV, and a symmetrical peak at about 2.1 eV, which are attributed to the O-2p valence and the localised U-5f^2 level, respectively. Examining the U-5f feature, at low oxygen pressure (2×10^{-5} mbar) the U-5f^2 peak lies at 2.1 eV, but with higher pressure it shifts to 1.4 eV, where it is found in stoichiometric $UO_{2.0}$ [19]. The shift is similar to that observed for the U-4f oxide lines, and is due to the further oxidation of the n-type UO_{2-x}. No further oxidation was observed for a partial pressure higher than 1×10^{-4} mbar, only a slight broadening of the peaks.

Both core level and valence band spectra show oxygen incorporation in the films to be divided into three regimes (Fig. 3). Region 1 corresponds to the transformation of U metal into UO_{2-x} resulting in an increase in

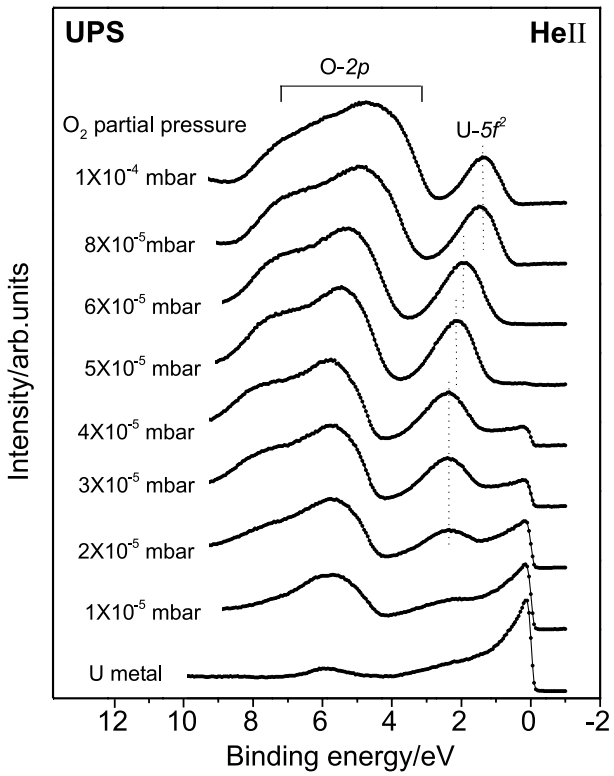

Fig. 2. UPS-He^{II} study of UO_x as a function of O_2 partial pressure.

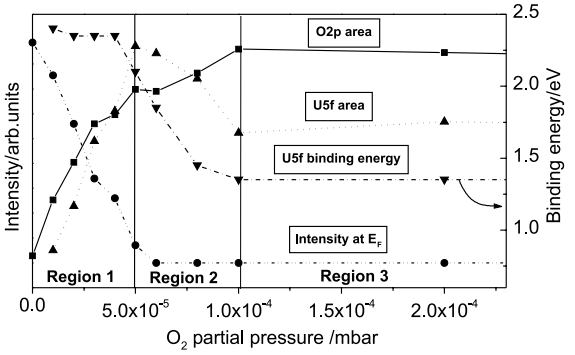

Fig. 3. Evolution of the UPS spectral features with the O_2 partial pressure.

localised 5f electrons and a decrease in the intensity at the Fermi level. At low oxygen partial pressures up to 5×10^{-5} mbar, all the intensities and areas vary linearly with the oxygen partial pressure. The formation of UO_{2-x} proceeds via simultaneous deposition of U and UO_{2-x} clusters and chemisorption of oxygen on the residual reactive U sites. Later (in region 2) the entire surface is covered by $UO_{2-x,}$ and further reaction of oxygen results in the transformation of UO_{2-x} into UO_2, causing a decrease of the localised U-5f intensity and the coherent binding energy shift of all emission lines. This further oxidation is induced by the reaction of molecular oxygen and was observed only at low temperature. At high temperature (573 K) only UO_{2-x} is formed. This is attributed to the decrease of the oxygen sticking probability on the surface. An alternative explanation, which is the diffusion of oxygen into the bulk, can be ruled out for such thin films of 5 nm, that have no significant interior volume to absorb oxygen. The gold substrate, indeed, is inert and cannot act as oxygen buffer. Region 3 corresponds to the saturation of oxygen, and shows the low reactivity of oxygen towards a UO_2 surface. The same oxidation behaviour has been observed for bulk U metal exposed to oxygen [20]. The development of higher oxides of uranium beyond UO_2 was not observed for sputter deposition between room temperature and 573 K. It is unlikely that deposition at higher substrate temperatures would yield higher oxidation states, because the temperature of the plasma during the deposition is much higher than that of the substrate, and increased substrate temperature results in low oxygen sticking probability. The transformation of UO_2 to UO_{2+x} is slower compared to the oxidation of U metal to UO_2. A uranium metal surface exposed to 60 L of oxygen at 300 K [20] is oxidised to UO_2. In comparison, the exposure to 1 Torr of oxygen for 120 h at room temperature is necessary for the formation of UO_{2+x} with $x \sim 0.06$ [21]. Exposure of a UO_2 thin film to 5000 L of oxygen does not show any change in the valence band spectra. Formation of higher uranium oxides requires higher oxygen partial pressures which is not possible for our deposition experiments, because at a critical threshold ($\sim 1 \times 10^{-3}$ mbar), the target itself oxidises. This results in the formation of an insulating or semiconducting oxide overlayer which disrupts the DC plasma. This effect is not observed, for example, in the case of uranium nitride preparation by reactive sputtering in Ar/N_2 or even pure N_2 [15]. Surface nitrides formed on the target have a metallic character and do not disturb the plasma. One possibility to produce higher oxides is to create strong local oxidation conditions on the substrate surface compared to the target, e.g., by adding an oxidation catalyst (Cs) to the film [12,22].

XRD measurements were performed on UO_2 thin films deposited on a glass substrate. The diffraction pattern shows a cubic structure with a lattice parameter of 5.47 ± 0.05 Å which is consistent with the formation of stoichiometric $UO_{2.0}$. It is also evident that the films are not amorphous, as sometimes observed for sputter-deposited films [23]. In spite of the fact that an amorphous substrate may suppress crystalline ordering in the film, XRD measurements of deposits on polycrystalline (Au disc), monocrystalline (Si) and amorphous (glass) substrates yield the same diffraction pattern. The type of substrate does not appear to influence the crystallinity of the film in our case. The microstructure of a material may affect the electrochemical behaviour, therefore the polycrystalline character of the thin films is important when the thin films are to be used as a simulation of fuel for electrochemical studies.

3.2. AC impedance measurements

The UO_2 thin films have been characterised by ac impedance measurements. The interpretation of the impedance data can be done using a model (equivalent electrical circuit) composed of resistance, capacitance or other elements as constant phase elements (CPE). Each element of the proposed circuit is associated with particular physical properties (e.g., electrode resistance, film layer capacitance) and chemically influenced properties (e.g., polarisation resistance, double layer capacitance) of the system.

For non-irradiated UO_2 fuel electrodes, equivalent circuits were proposed [6,11] consisting of two RC circuits in series (Fig. 4). The first part describes the electric and dielectric behaviour of the electrode with a resistance R_{el}, in parallel with a capacitance C_{el}. In case of a thin film supported on gold substrate, the resistance and the capacitance of the gold substrate (e.g., $R_{Au} = 1 \times 10^{-7}$ Ω) are negligibly small compared to UO_2 (e.g., 40 kΩ for 2 mm thick electrode). The second RC circuit simulates the electrode–solution interface with the polarisation resistance (R_{pol}) in parallel with the double layer capacitance (C_{dl}) followed by the resistance R_Ω

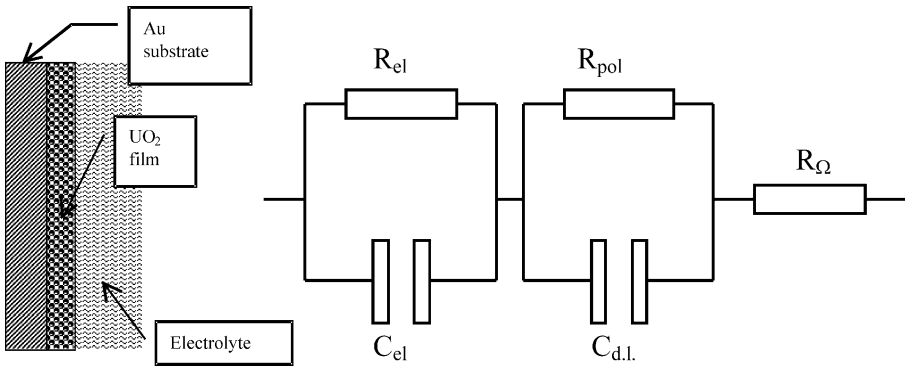

Fig. 4. Equivalent circuit of a film electrode. The capacitance and resistance of the electrode are represented by C_{el} and R_{el}, R_{pol} the polarisation resistance of the electrode and electrolyte interface and C_{dl} the double layer capacitance.

which includes the resistance of the electrolyte and of the electrical connections. The electrode properties and geometry influence the values of the parameters in the equivalent circuit significantly. The main distinction between a film UO_2 electrode and a bulk UO_2 electrode arises from the difference in thickness. Typically, the film is 1 μm thick, compared to the 2 mm thick bulk electrode, and this changes the values in the equivalent circuit related to geometry of the electrode (R_{el} and C_{el}). Under ideal conditions, the resistance of the electrode could be obtained from the electrical conductivity of UO_2 ($\kappa \sim 10^{-5}$ Ω^{-1} cm^{-1} [25]) using

$$R_{el} = d(\kappa A_{el})^{-1}.$$

For an electrode surface area (A_{el}) of about 0.5 cm^2 and a thickness (d) of 1 μm, the resistance of the electrode is about 20 Ω (compared to 40 kΩ for a 2 mm thick electrode). Therefore no correction to the applied potential is necessary to compensate the potential drop (IR). The electrode capacitance is also affected by the thickness of the electrode. Assuming that the electrode behaves as an ideal capacitor, the capacitance can be estimated using the equation

$$C_{el} = \varepsilon_0 \varepsilon A_{el} d^{-1}$$

with the dielectric number (ε) for UO_2 of 10 [26] and the surface area and thickness given above. An electrode capacitance (C_{el}) of about 5 nF is obtained for a film electrode, whereas a value of ~3 pF is obtained for a 2 mm thick electrode. A typical value for C_{dl} is between 1 and 100 μF cm^{-2}. At open-circuit potential, a low corrosion rate is expected (~1 mg d^{-1} m^{-2} [24]), which is related to a high polarisation resistance of 10 MΩ. Fig. 5 shows Bode-plots of the calculated impedance spectra of a film and a bulk electrode. In the frequency range from

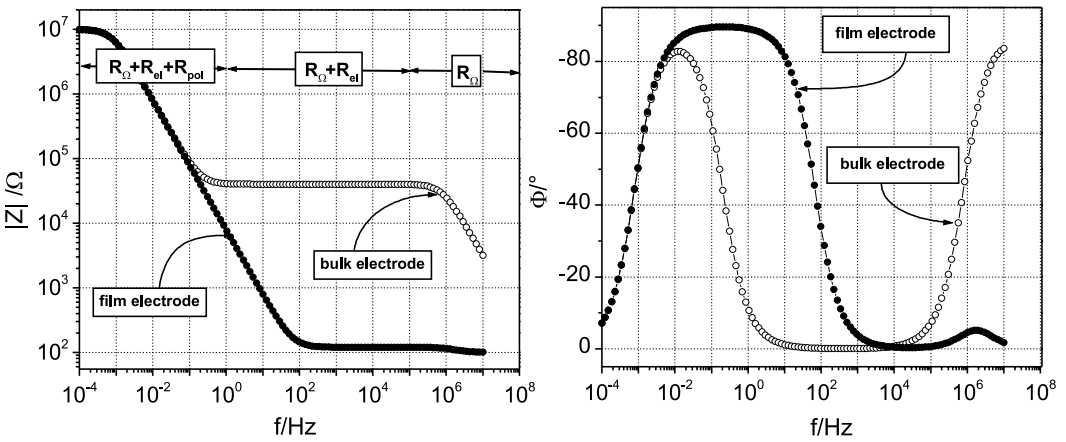

Fig. 5. Calculated impedance spectra for a film (1 μm thick and 0.5 cm^2 as electrode area) and bulk electrode (2 mm thick and 0.5 cm^2) using the equivalent circuit shown in Fig. 4. (For the film electrode, the values of the equivalent circuit are: $R_\Omega = 100$ Ω, $R_{el} = 20$ Ω, $C_{el} = 5$ nF, $R_{pol} = 10$ MΩ and $C_{dl} = 20$ μF. For the bulk electrode: $R_\Omega = 100$ Ω, $R_{el} = 40$ kΩ, $C_{el} = 5$ pF, $R_{pol} = 10$ MΩ and $C_{dl} = 20$ μF.)

10^6 Hz down to 10 Hz, the absolute value of the impedance ($|Z|$) is determined by the sum of R_Ω and R_{el} where R_Ω is negligibly small. In the lower frequency part (<1 Hz) the impedance value is related to the polarisation resistance, because R_Ω and R_{el} can be neglected compared to R_{pol} in this frequency range. In the case of a film electrode, the low electrode resistance (20 Ω) can be seen on the Bode-plot by the drop of the impedance value in the higher frequency range (>100 Hz) compared to a bulk electrode. Therefore, the polarisation resistance, which is related to the chemical process (e.g., dissolution process), is highlighted.

The use of a double RC equivalent circuit is limited to the ideal situation where only the UO_2 layer is in contact with the electrolyte. However porosity and the presence of defects may lead to penetration by the electrolyte into the gold substrate (Fig. 6). Thus the impedance measurements of the working electrode will not only be due to the electrochemical behaviour of UO_2 but will also feature a contribution from the gold substrate. The electrochemical behaviour of gold electrodes had been studied in the past [27–29]. In the presence of anions such as Cl^- or Br^-, adsorption phenomena have been observed on the gold surface [28]. Therefore a circuit is added in parallel to the previous double RC equivalent circuit of UO_2. The new components simulate the electrolyte/gold interface. The gold contribution is represented by the polarisation resistance of the metal ($R_{met,pol}$) in series with the capacitance of the adsorbed anion layer ($C_{met,ads}$) and an impedance element as a Warburg impedance ($Z_w(\omega) = A_w(j\omega)^{-1/2}$) describing diffusion through the electrolyte and the thin film of the adsorbed anions. This branch is in parallel with the double layer capacitance ($C_{met,dl}$) of the electrolyte/gold interface.

Impedance spectra ($|Z|$ vs. frequency and phase angle vs. frequency) of UO_2 film (1.6 μm thick) and UO_2 bulk electrode (1 mm thick) are shown in Fig. 7(a). The thin film electrode spectra are fitted by the equivalent electrical circuit shown in Fig. 6. Due to the non-ideal behaviour of the capacitance, a constant phase element (CPE) must be taken into consideration. The leaching rate is calculated from the polarisation resistance using the Stern–Geary equation [30] and Faraday's law

$$I_{corr} = BR_{pol}^{-1},$$
$$v_{corr} = MI_{corr}(ZFA_{el})^{-1},$$

where M is the atomic mass of UO_2 (270.03 g mol^{-1}), Z is the number of electrons exchanged in the dissolution reaction, two electrons in this case. A_{el} is the surface area of the electrode. B is calculated from the anodic (b_a) and cathodic (b_c) Tafel slopes ($B \sim 25$ mV [24]). Using values for natural UO_2 derived from the literature sources, the polarisation resistance derived from the fitting of the equivalent circuit to the curve is 6.8 MΩ for electrode of 0.5 cm^2 surface area. A leaching rate v_{corr} of ~8.9 mg d^{-1} m^{-2} has been found for these conditions (0.1 M KCl, oxidising, pH = 5.7, stirred solutions).

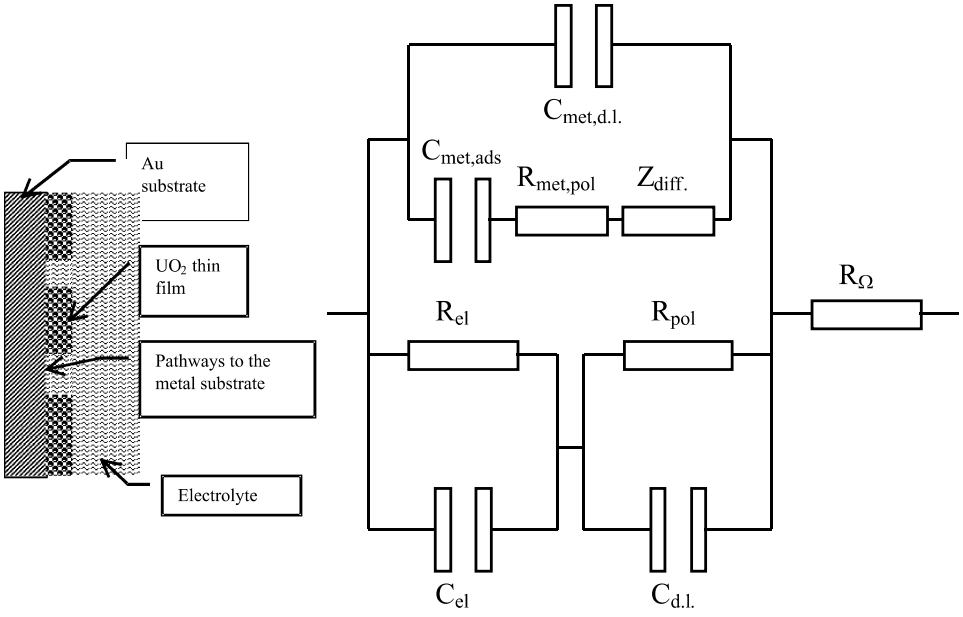

Fig. 6. Equivalent circuit of film electrodes with conductive pathways between the substrate and the electrolyte solution. An additional polarisation resistance $R_{met,pol}$ and double layer capacitance $C_{met,dl}$ are correlated to the metal corrosion. The adsorption capacitance C_{ads} and the diffusion impedance Z_{diff} are related to anions' electrosorption phenomena on the gold electrode.

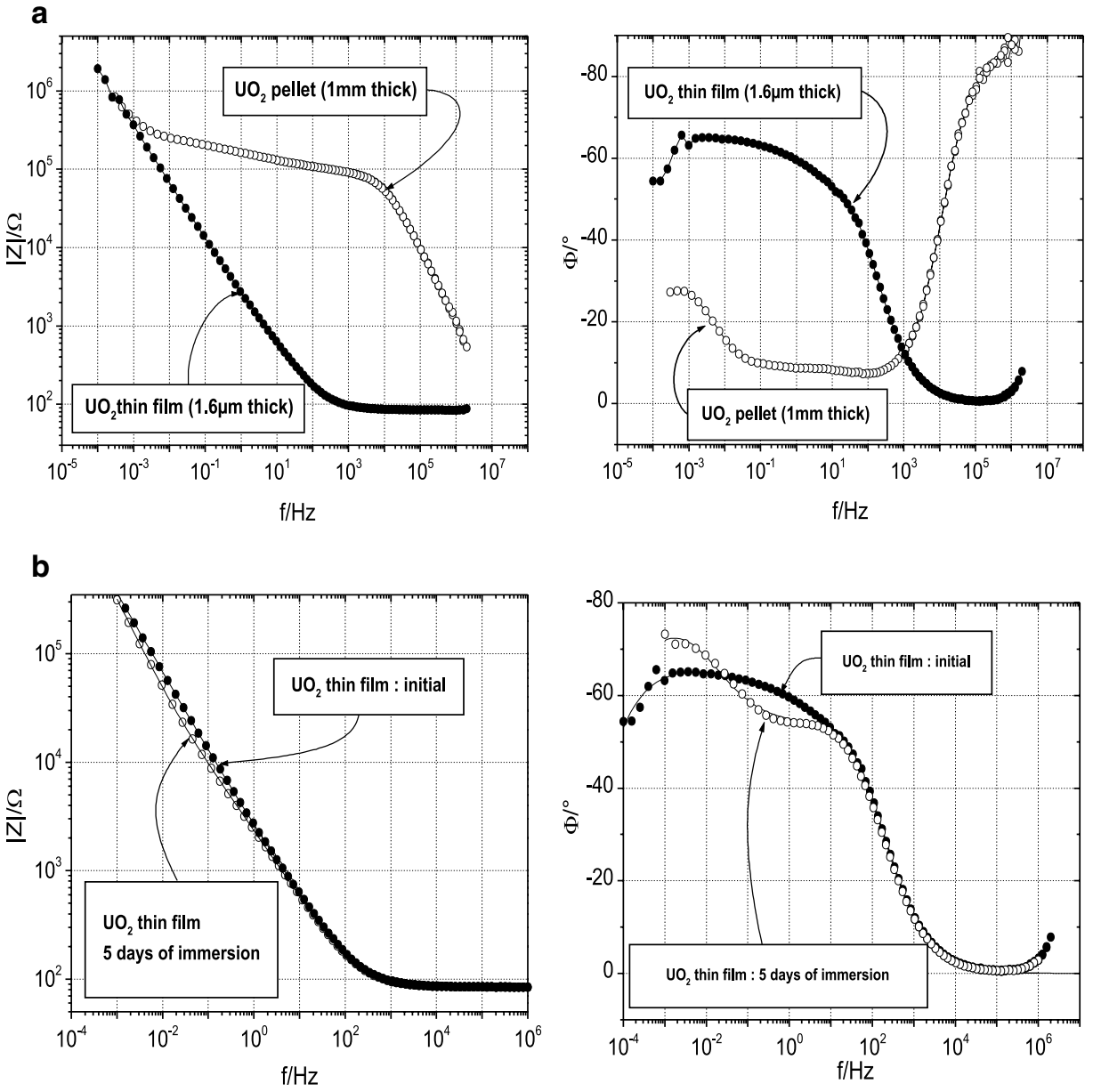

Fig. 7. (a) AC impedance spectra of UO_2 film and bulk electrodes performed in 0.1 M KCl aerated solution (pH $\sim$ 6, RT) at rest potential (measured 6 h before the start of the measurement). (b) AC impedance spectra of UO_2 thin film electrodes at 6 h after the immersion and after 5 days of immersion (0.1 M KCl, RT; pH = 6, rest potential).

Alternatively, the leaching rate was obtained from the free corrosion potential measured before the impedance measurement, using the calibration curve published in [24]. The value of $E_{corr} = 293$ mV_{SHE} corresponds to a leaching rate of 2.3 mg d^{-1} m^{-2}. The values found with the two different methods are thus in good agreement. Leaching rates between 1 and 17 mg d^{-1} m^{-2} are reported in [24] for unirradiated UO_2 in synthetic groundwater or 95% saturated NaCl.

After 5 days of immersion in 0.1 M KCl solution, the polarisation resistance derived by fitting increases by 1 order of magnitude (67 MΩ) (Fig. 7(b)). The corrosion rate decreases to 0.9 mg d^{-1} m^2. There are two possible explanations for this observation: firstly the formation of a secondary phase which blocks the dissolution or secondly by the rapid release of easily leached components followed by steady-state conditions.

3.3. Open-circuit measurements

Free corrosion potential measurements (Fig. 8) have been performed using UO_2 film electrodes in stirred and aerated 0.1 M KCl solutions at various pHs. The electrode was changed for each measurement and precathodised at -1300 mV_{SHE} for 5 min before switching to open circuit. Although gold-based electrodes have the least influence on the UO_2 corrosion potentials compared to steel or brass bases [24], nevertheless an influence is still observed in the impedance measurements because of its sensitivity to porosity penetrating into the substrate. For this reason open-circuit measurements on blank gold electrodes have been performed. These control measurements show a stable free corrosion potential value ($E_{corr,Au} = +150$ mV_{SHE}) at pH = 2 and 12. Therefore a change with the pH of the solution in E_{corr} measured on UO_2 film electrodes cannot be attributed to the formation of a mixed potential between the electrolyte/UO_2 and the electrolyte/gold interfaces. Fig. 8 shows that during the first hour the free corrosion potential quickly evolves to higher values. A slower development is then observed for longer exposures.

For a passive layer formation on metallic surfaces (e.g., Ti, Mo, Ta) [32], the following relation has been used to characterise the layer growth: $E_{corr} = A + B\log(t)$. The constants A and B are related to anodic and cathodic processes involved in the layer growth (e.g., related to the reaction rate constants, the transfer coefficients and the number of electrons exchanged). Therefore, a change of the slope in the E_{corr} vs. log(time) diagram indicates a change in the growth of a surface layer. All corrosion potential curves show at least two linear regions which are attributed to a two-step mechanism of film growth on the UO_2 surface: during the first 2 h of corrosion, a UO_{2+x} ($0 < x < 0.33$) film is formed. In the second step, the film further oxidises to hydrated U^{VI} species. Sunder and Shoesmith [31] have reported similar findings using pellet electrodes.

Free corrosion potentials of UO_2 thin films were measured at various pHs, and found to decrease with increasing pH. From the corrosion potentials the dissolution rates of UO_2 were deduced [2,24]. The leaching rates range from 5 (pH = 2) to 0.002 mg m^{-2} d^{-1} (pH = 12) (Table 1). A similar dependence has been obtained for bulk UO_2 [31]. It is seen that the thin film electrodes can be used to study the dissolution behaviour of UO_2.

3.4. Cyclic voltammetry measurements

In Fig. 9 cyclic voltammograms (CVs) are given for 1 μm thick UO_2 coated working electrodes in aerated and stirred 0.1 M KCl solutions at various pHs (pH adjusted by 1 M NaOH or 1 M HCl solutions). A cathodic potential of -1300 mV_{SHE} was applied for 2 min, before starting the measurements to reduce any higher oxides which may have formed on the surface (e.g., during contact with the atmosphere). The potential sweeps started at -1300 up to $+800$ mV_{SHE} and afterwards back to the cathodic potential of -1300 mV_{SHE}. The scan rate was 50 mV s^{-1}. The applied potential was not corrected for the IR drop due to the small electrode resistance as shown above by impedance measurements.

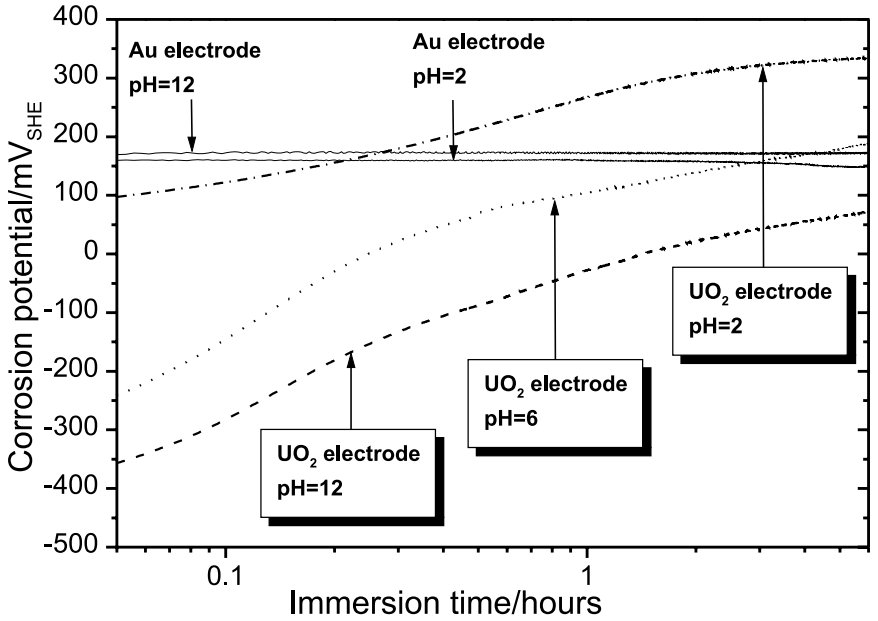

Fig. 8. Open-circuit measurements on UO_2 film electrode in 0.1 M KCl solution at various pHs (RT, aerated and stirred solution).

Table 1
Leaching rates of UO_2 thin films in 0.1 M KCl solution at various pHs. The leaching rates are calculated from the calibration curve published in [24]

pH solution	${}^{max}E_{corr}$ (mV_{SHE})	Leaching rate (mg d^{-1} m^{-2})
2	336 ± 15	5 ± 3
6	189 ± 15	0.07 ± 0.03
12	70 ± 15	0.002 ± 0.002

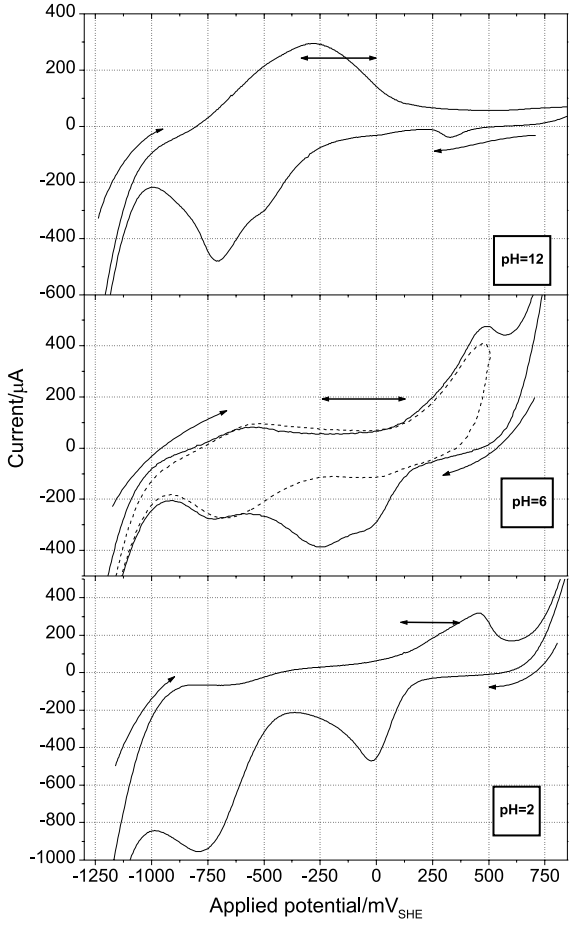

Fig. 9. Cyclic voltammetry measurements on a UO_2 film electrode in 0.1 M KCl aerated and stirred solution at various pHs (RT, 50 mV s^{-1}) (dotted line at pH = 6 is a curtailed sweep to +500 mV_{SHE}).

As already described by Sunder et al. [4], the dissolution mechanism is different for an acidic than for a neutral or alkaline solution. CVs (Fig. 9) at various pH values also show changes in the dissolution behaviour.

The horizontal bars on the CVs in the Fig. 9 indicate the potential regions for the film growth under open-circuit conditions taken from the free corrosion potential measurements (Fig. 8). Therefore the anodic shoulder between −500 and 0 mV_{SHE} observed clearly for the voltammogram at pH = 12 and slightly at pH = 6 must be related to the formation of the higher oxide layers. Sunder et al. [31] assigned cathodic peaks between −670 and −750 mV_{SCE} (−430 to −510 mV_{SHE}) to the reduction of $UO_{2.33}$ to UO_{2+x}, and between −830 and −870 mV_{SCE} (−590 to −630 mV_{SHE}) to the reduction of $UO_{2.67}$ to UO_{2+x}, and finally between −100 and −300 mV_{SCE} (+140 to −60 mV_{SHE}) to the more easily reduced secondary phase $UO_3 \cdot xH_2O$ to UO_{2+x}.

We observed two cathodic peaks at pH = 12 at −470 and −700 mV_{SHE} which can be attributed to reduction of $UO_{2.67}$ and $UO_{2.33}$ to UO_{2+x}. Two additional cathodic peaks are present at pH = 6 at ~0 and ~ −250 mV_{SHE} Sunder et al. [4] claim the presence of a layer containing U^{VI} species on the electrode surface which can act as a precursor to either the formation of oxide films (secondary phase: $UO_3 \cdot xH_2O$) or dissolved uranyl species present as an adsorbed UO_2^{2+} layer. These two cathodic peaks observed on the CV at pH = 6 were assigned to the reduction of the U^{VI} species (Fig. 9). This observation is confirmed by the lower cathodic potential needed to reduce them, and also the disappearance of the peaks if the anodic sweep is stopped at a lower value (before +500 mV_{SHE}, dotted line), before the corresponding electrochemical oxidation or dissolution could occur. Therefore the dissolution model developed by Shoesmith [2] for neutral and alkaline solutions and consisting of the following reactions ($UO_2 \rightarrow UO_{2+x} \rightarrow UO_{2.33} \rightarrow UO_2^{2+} \rightarrow UO_3 \cdot xH_2O$) also fit our data. Although the shift in the main anodic peak in going from pH = 12 to pH = 6 is bigger than in their case. In the case of an acidic solution, a distinct change of behaviour has also been observed in the past [4]. The free corrosion potential at pH = 2 reaches a steady-state value more rapidly (Fig. 8). The potential region of oxide film growth is narrower and occurs at a more positive potential value in acidic solution than in neutral solutions. Also the anodic shoulder present on the voltammograms at pH = 6 and pH = 12 is no longer present for the acidic solution. The thermodynamic stability boundary between $UO_{2.33}$ and UO_2 based on the ΔG_f^0 of $UO_{2.33}$ [33] was determined to be approximately +400 mV_{SHE} for pH = 2 and therefore is higher than free corrosion potential measured in 0.1 M KCl pH = 2. This means that the $UO_{2.33}$ layer is thermodynamically unstable and will not be formed under these conditions. On the CV, the cathodic peak at ~0 mV_{SHE} is assigned to the reduction of a U^{VI} species layer on the electrode surface. The electrochemical oxidation/dissolution of UO_2 in acidic solutions seems to differ from that in neutral solutions where the oxidation of an overlayer of $UO_{2.33}$ leads afterwards to the formation of an intermediate U^{VI} species. In acidic solution $UO_{2.33}$ is no longer formed directly on the anodic sweep, but higher oxides instead

(such as $UO_{2.67}$). Soluble U^{VI} species can then also be formed because of the high dissolution rate under acidic conditions [31,34]. Typically, this is a species such as UO_2^{2+} which can also adsorb on the surface or form $UO_3 \cdot xH_2O$ or other hydrolysed products. These are apparently not particularly stable [35] and are reduced on the return sweep at approximately 0 mV_{SHE} to a state such as $UO_{2.33}$. The cathodic sweep at the more negative potential (-760 mV_{SHE}) in pH = 2 solution could be attributed to the reduction of lower oxides (e.g. $UO_{2.33}$) to initial oxidation of UO_{2+x}. This peak could also have contributions from the reduction of O_2 as noted by Hocking et al. [36]. The prominence of the anodic peaks at $+500$ mV_{SHE} for acid (pH = 2) and neutral (pH = 6) conditions suggests a relatively high specific surface area, that is a certain degree of porosity in the films. Examination of the thin films before cyclic voltammetry by optical microscopy revealed a slight level of defects and/or porosity. This would obviously increase during the anodic sweep and increase the specific surface area of the film electrode compared to solid surfaces (such as single crystal UO_2). Nevertheless with porous surfaces such as UO_2 pellets a similar effect would be seen. This is confirmed by the impedance results where inclusion of the gold/electrolyte interface is necessary to obtain the best fitting of the measurements.

4. Conclusions

The dissolution behaviour of UO_2 films was studied by electrochemical methods. The films were produced by reactive sputtering and their composition was confirmed by XPS, UPS and XRD. The characterisation of films at various oxygen partial pressures showed that deposition occurs in a two-step process, consisting of the oxidation of metallic U into UO_{2-x} and the further oxidation of UO_{2-x} into UO_2.

Electrochemical studies of UO_2 film electrodes give similar results as those obtained on UO_2 pellets. The corrosion rate based on the polarisation resistance and the mechanism of corrosion are comparable for both film and bulk electrodes. AC impedance measurements confirm that the resistance of the film electrode is much lower than for pellet electrodes, which means that the IR drop for cyclic voltammetry or open-circuit measurements can be neglected.

Cyclic voltammetry showed that the dissolution mechanism found for natural UO_2 pellets can also be applied to film electrodes. In both cases the same dependence on the pH of the electrolyte is observed. In acidic solutions $UO_{2.33}$ is no longer formed, in contrast to alkaline solutions, but a layer of U^{VI} species is present on the electrode surface.

Several applications of this technique can therefore be foreseen. It is also possible to produce films of other materials and study their reactivity in various aqueous environments. By co-depositing other species as a simulation of fission products, the influence of fission products on the dissolution behaviour of fuel can be electrochemically investigated under known and controlled conditions, thus bridging the gap between pure UO_2 and complex spent fuel.

Acknowledgements

We thank to S. Van Den Berghe from SCK·CEN for fruitful discussions.

References

[1] D.W. Shoesmith, S. Sunder, J. Nucl. Mater. 282 (2000) 1.
[2] D.W. Shoesmith, S. Sunder, An electrochemistry-based model for the dissolution of UO_2, Atomic Energy of Canada Ltd, Report, AECL-10488, 1991.
[3] D.W. Shoesmith, W.H. Hocking, B.M. Ikeda, F. King, J.J. Noel, S. Sunder, Can. J. Chem. 75 (1997) 1566.
[4] S. Sunder, D.W. Shoesmith, N.H. Miller, J. Nucl. Mater. 244 (1997) 66.
[5] G. Marx, J. Engelhardt, F. Feldmaier, M. Laske, Radiochim. Acta 74 (1996) 181.
[6] P.-M. Heppner, D.H. Wegen, G. Marx, Radiochim. Acta 58&59 (1992) 21.
[7] P. Trocellier, C. Cachoir, S. Guilbert, J. Nucl. Mater. 256 (1998) 197.
[8] L.H. Johnson, D.W. Shoesmith, G.E. Lunansky, M.G. Bailey, P.R. Tremaine, Nucl. Technol. 56 (1992) 238.
[9] L.H. Johnson, D.W. Shoesmith, in: W. Lutze, R.C. Ewing (Eds.), Radioactive Waste Forms for the Future, Elsevier, Amsterdam, 1988.
[10] D.W. Shoesmith, S. Sunder, M.G. Bailey, N.H. Miller, J. Nucl. Mater. 227 (1996) 287.
[11] P.D.W. Bottomley, D.H. Wegen, M. Coquerelle, J. Nucl. Mater. 238 (1996) 23.
[12] V. Volkovich, T.R. Griffiths, D.J. Fray, M. Fields, P.D. Wilson, J. Chem. Soc., Faraday Trans. 92 (1996) 5059.
[13] G.C. Allen, J.A. Crofts, M.T. Curtis, P.M. Tucker, D. Chadwick, P.J. Hampson, J. Chem. Soc. Dalton 3 (1974) 1296.
[14] G.C. Allen, P.M. Tucker, J.W. Tyler, J. Phys. Chem. 86 (1982) 224.
[15] L. Black, F. Miserque, T. Gouder, L. Havela, F. Wastin, J. Rebizant, J. Alloys Compd. 315 (2001) 36.
[16] F. Greuter, E. Hauser, P. Oelhafen, H.J. Güntherrodt, B. Reihl, O. Vogt, Physica B 102 (1980) 117.
[17] T. Gouder, PhD thesis, Facultés Universitaires Notre-Dame de la Paix, Namur, Belgium, 1987.
[18] G.C. Allen, P.M. Tucker, J.W. Tyler, J. Phys. Chem. 86 (1982) 224.
[19] N. Beatham, A.F. Orchard, G. Thornton, J. Electron Spectrosc. Relat. Phen. 19 (1980) 205.
[20] T. Gouder, C. Colmenares, J.R. Naegele, J. Verbist, Surf. Sci. 235 (1989) 280.

[21] G.C. Allen, P.A. Tempest, J.W. Tyler, J. Chem. Soc., Faraday Trans. 84 (11) (1988) 4049.
[22] F. Miserque, T. Gouder, S. Van Den Berghe, D.H. Wegen, P.D.W. Bottomley, in: 5th International Conference on Nuclear and Radiochemistry, Pontresina, Switzerland, 2000.
[23] K.H.J. Buschow, Handbook on the Physics and Chemistry of Rare Earths, vol. 7, North-Holland, Amsterdam, 1984, p. 278.
[24] Source term for performance assessment of spent fuel as a waste form, Project Report, Euratom, Eur19140, 2000.
[25] Belle, Uranium Dioxide: Properties and Nuclear Applications, Washington, DC, 1961.
[26] Gmelin, Uranium Suppl. C5 (55) (1986).
[27] T. Pajkossy, T. Wandlowski, D.M. Kolb, J. Electroanal. Chem. 414 (1996) 209.
[28] D. Eberhardt, E. Santos, W. Schmickler, J. Electroanal. Chem. 419 (1996) 23.
[29] A. Hamelin, J. Electroanal. Chem. 142 (1982) 395.
[30] M. Stern, A.L. Geary, J. Electrochem. Soc. 104 (1957) v56.
[31] S. Sunder, D.W. Shoesmith, R.J. Lemire, M.G. Bailey, G.J. Wallace, Corros. Sci. 32 (4) (1991) 373.
[32] A.G. Gad-Allah, H.A. Abd El-Rahman, Corrosion-NACE 43 (11) (1987) 698.
[33] I. Grenthe, J. Fuger, R.J.M. Konings, R.J. Lemire, A.B. Muller, C. Nguyen-Trung Cregu, H. Wanner, Chemical Thermodynamics of Uranium, North-Holland, Amsterdam, 1992.
[34] S. Sunder, L.K. Strandlund, D.W. Shoesmith, Electrochem. Acta 43 (1998) 2359.
[35] D.W. Shoesmith, S. Sunder, W.H. Hocking, in: J. Lipkowski, P. Ross (Eds.), Electrochemistry of Novel Materials, VCH, New York, 1994.
[36] W.H. Hocking, J.H. Betteridge, D.W. Shoesmith, J. Electroanal. Chem. 379 (1994) 339.